Journal of Power Sources 225 (2013) 163–171

Contents lists available at SciVerse ScienceDirect

Journal of Power Sources

journal homepage: www.elsevier.com/locate/jpowsour

Carbon monoxide, methanol and ethanol electro-oxidation on Ru-decorated carbon-supported Pt nanoparticles prepared by spontaneous deposition

Amado Velázquez-Palenzuela, Enric Brillas, Conchita Arias, Francesc Centellas, José Antonio Garrido, Rosa María Rodríguez, Pere-Lluís Cabot*

Laboratori d'Electroquímica dels Materials i del Medi Ambient, Departament de Química Física, Universitat de Barcelona, Martí i Franquès 1-11, 08028 Barcelona, Spain

HIGHLIGHTS

- ► Ru(Pt)/C electrocatalysts were synthesized using spontaneous deposition.
- ► The Ru species deposition was fitted to a Roginsky–Zeldovich–Elovich kinetics.
- ► The maximum activity was achieved for coverage (θ) of about 0.25.
- ► The ECSA increase for $\theta < 0.25$ was related to deposition of reducible Ru oxides.
- ► The Tafel slopes were related to the coverage by Ru species.

ARTICLE INFO

Article history:
Received 8 June 2012
Received in revised form
5 October 2012
Accepted 8 October 2012
Available online 22 October 2012

Keywords:
Pt–Ru nanoparticles
Electrocatalysis
CO stripping
Methanol oxidation reaction
Ethanol oxidation reaction
Spontaneous deposition

ABSTRACT

Carbon-supported Pt nanoparticles (Pt/C) were modified by spontaneous deposition of Ru species in 0.1 M $HClO_4$ solutions with different Ru concentrations and treatment duration. Cyclic voltammetry (CV) of thin-layer electrodes in 0.5 M H_2SO_4 allowed determining the coverage θ of Pt by the Ru deposits. The CO oxidation activity of the Ru-decorated Pt specimens (Ru(Pt)/C) was evaluated by CO stripping measurements in the same background electrolyte. The activity towards methanol and ethanol oxidation was tested using CV in 0.5 M H_2SO_4 with 1.0 M CH_3OH or 1.0 M CH_3CH_2OH. A promotional effect of all the anodic reactions due to the introduction of Ru species was detected, with a significant reduction of the overpotential in all cases. The optimum coverage for achieving the best CO oxidation activity and the highest current for the oxidation of these alcohols was found around $\theta = 0.20–0.30$, indicating the involvement of CO as intermediate in the oxidation pathway of both, methanol and ethanol. The observed activation was mainly assigned to the deposited hydrous Ru oxide (RuO_xH_y). The Tafel slopes were analyzed and discussed on the basis of the presence of Ru species and the proposed mechanism for each oxidation reaction.

1. Introduction

Recently, an extensive research on polymer electrolyte fuel cells (PEFCs) has been made owing to their excellent performance as energy supplier systems with high conversion capability, low operating temperature, and scarce production of contaminant exhaust [1]. Although hydrogen is the most employed fuel in this kind of devices because it presents fast oxidation kinetics on Pt-based electrocatalysts [2], PEFCs operating with low-molecular weight organic molecules and without a previous reforming step have attracted large research efforts [3]. Thus, the direct methanol [4–13] and direct ethanol [14–20] fuel cells, DMFCs and DEFCs, respectively, use easy-handling liquid electrolytes, the production cost of the fuel is low, and they can be easily incorporated in portable electronic systems. Both DMFCs and DEFCs share the problem of the CO generation as intermediate in the corresponding oxidation pathways to CO_2, which poisons the Pt active sites [9,16]. This problem can be solved using Pt–Ru instead of pure Pt since the presence of Ru allows achieving higher tolerance against the CO poisoning, thereby improving the electrocatalytic properties for methanol (MOR) and ethanol (EOR) oxidation reactions [7]. This enhancement of the anodic reactions is generally explained on the basis of a bifunctional mechanism that occurs through the participation of oxygenated species formed on Ru atoms by water discharge at lower potential than on Pt atoms [8]. As additional

* Corresponding author. Tel.: +34 93 4039236; fax: +34 93 4021231.
E-mail address: p.cabot@ub.edu (P.-L. Cabot).

0378-7753/$ – see front matter © 2012 Elsevier B.V. All rights reserved.
http://dx.doi.org/10.1016/j.jpowsour.2012.10.012

contribution, a ligand effect has also been established, based on the alteration of the Pt electronic structure that originates a weakening of the Pt–CO bond [21].

In view of the superior activity of bimetallic electrocatalysts, research efforts have been concentrated in the synthesis of carbon-supported Pt–Ru alloy nanoparticles (Pt–Ru/C) because the alloyed systems allow a closer contact between the Pt and Ru atoms [22,23]. However, there is no consensus about the optimum Ru composition which causes the maximum activity for the fuel oxidation, principally in the case of methanol. Thus, Aricò et al. [4] found the maximum activity with a composition of 50 at% Ru when analyzing the methanol oxidation on unsupported Pt–Ru nanoparticles. In contrast, Gasteiger et al. [7] reported a lower optimum Ru surface composition of 10 at% at 25 °C, changing to 30 at% at 60 °C, for smooth polycrystalline Pt–Ru alloys. Frelink et al. [6] also reported a most favorable surface Ru content of 15 at% for the MOR on co-deposited Pt–Ru electrodes characterized with an electrochemical quartz crystal microbalance. The disparity of results can be explained attending the different Ru speciation on the Pt surface, i.e., Ru can appear as metallic Ru, ruthenium oxide (RuO_2) or hydrous ruthenium oxide (RuO_xH_y) [24,25]. According to Rolinson et al. [26], the different Ru species can be involved in the promotional effect of the CO and the carbonaceous fuel oxidation with dissimilar activation result.

The above considerations indicate that the knowledge of the actual Ru surface composition is essential in order to compare Pt–Ru electrocatalysts with different Ru fractions. For this purpose, a trustworthy strategy for the preparation of Pt electrocatalysts with an accurate control of the surface coverage by the Ru species has been based on the spontaneous deposition technique [27–32]. The corresponding XPS analyses have shown that the main species formed during the spontaneous deposition are Ru oxides [29]. This procedure has been predominantly used for the Ru decoration of Pt (*hkl*) electrodes for the MOR evaluation, where the Ru-modified Pt (111) face electrode has been found as the most favorable electrocatalytic surface [28,29]. Thus, Iwasita et al. [28] reported a wide optimum Ru surface composition ranging from 10 to 40 at% for the MOR at Ru deposits on Pt (111) surface. However, less is known about Ru spontaneous deposition on Pt nanoparticles that lead to applicable electrocatalysts for PEFC anodes. Waszczuk et al. [32] synthesized Ru-decorated unsupported Pt nanoparticles and found a more suitable Ru packing density of 0.4–0.5 when they were tested for the MOR. In contrast, when Maillard et al. [31] compared the MOR on Ru-modified carbon-supported Pt nanoparticles prepared by spontaneous or electrochemical deposition, optimum surface coverages of 10 and 20 at%, respectively, were found. As far as we know, no previous work has been focused on the analysis of the coverage of carbon-supported Pt nanoparticles by Ru species towards the CO oxidation and its connection with MOR and EOR.

This paper presents the electrochemical analysis of Ru-modified Pt nanoparticles supported on Vulcan XC-72 for the MOR prepared by means of the spontaneous deposition technique (Ru(Pt)/C electrocatalysts). For this purpose, the thin-layer electrode technique, consisting in the deposition of aliquots of electrocatalyst aqueous suspensions on glassy carbon (GC) electrodes, was performed. The Ru deposition process was characterized and the influence of the Ru precursor concentration as well as the duration of the modification step was investigated. The surface modification of the electrocatalyst and the kinetic parameters for the CO oxidation, MOR and EOR in acid media were studied by cyclic voltammetry. The influence of the coverage by the Ru species on the electrocatalytic ability was evaluated to determine the optimum compositions for such anodic reactions.

2. Experimental

2.1. Materials and reagents

High performance (HP) 20 wt% Pt nanoparticles supported on carbon Vulcan XC-72 (Pt/C electrocatalyst, actual analysis giving 19.6 wt% Pt on carbon) was acquired from E-Tek. GC disk electrodes of 3 mm diameter were provided by Metrohm. Hydrous ruthenium chloride ($RuCl_3 \cdot xH_2O$, Ru content 38 wt%) and analytical grade 70% $HClO_4$ from Merck were used for the preparation of $RuCl_3/HClO_4$ solutions. 96% H_2SO_4, 99.9% methanol and 99.9% ethanol were of analytical grade from Merck and Panreac. All solutions were prepared with high-purity water obtained from a Millipore Milli-Q system (resistivity $>$ 18 MΩ cm). Ar gas was Linde 5.0 (purity $\geq$ 99.999%) and CO gas was Linde 3.0 (purity $\geq$ 99.9%).

2.2. Electrode preparation

Aqueous slurries with 3.0 mg ml^{-1} of Pt/C electrocatalyst were prepared by sonicating for 45 min appropriate amounts of catalyst powder and ultrapure water. Afterward, 3.0–3.5 μl of the well dispersed ink was deposited by means of a digital micropipette on the surface of the GC disk electrode. The prepared electrodes were dried under the heat of a lamp for 15 min and further, they were coupled to an Ecochemie Autolab RDE to be used as working electrodes of the spontaneous deposition process and the electrochemical measurements. The final Pt loadings on the GC surface were always 30 μg cm^{-2}. Prior to the ink deposition, the GC tip was consecutively polished with aluminum oxide pastes of 0.3 and 0.05 μm (Buehler Micropolish II deagglomerated α-alumina and γ-alumina, respectively) on a Buehler PSA-backed White Felt polishing cloth until achieving a mirror finish, being rinsed with Millipore Milli-Q water in an ultrasonic bath between the polishing steps. The coverage of GC by the Pt/C ink approached 100% in all cases.

2.3. Electrochemical measurements

The electrochemical experiments were performed with a Metrohm 200-ml thermostated double wall three-electrode glass cell and an Ecochemie Autolab PGSTAT100 potentiostat–galvanostat with computerized control by Autolab Nova 1.5 software. A Pt rod of 3.78 cm^2 apparent area was used as the auxiliary electrode and a double junction Ag|AgCl|KCl (saturated) electrode ($E_{ref} = 0.199$ vs SHE) was employed as the reference electrode. All potentials given in this work are referred to the SHE scale. The measurements started with a potential cycling step in 0.5 M H_2SO_4 electrolyte, which was firstly deaerated by bubbling Ar for 30 min. For this purpose, 10 cyclic voltammograms at 0.10 V s^{-1}, 5 more at 0.05 V s^{-1}, and 3 more at 0.02 V s^{-1} between 0.02 and 0.65 V, were consecutively performed under Ar atmosphere at 25.0 °C. The recorded cyclic voltammograms were practically quasi-steady after the second cycle, evidencing the stability and cleanness of the prepared electrodes.

CO stripping measurements were conducted in 0.5 M H_2SO_4 between 0.02 and 0.98 V at 0.02 V s^{-1} and 25.0 °C under Ar atmosphere. CO was previously bubbled through the solution for 15 min, keeping the electrode potential at 0.10 V to assure its complete adsorption. The CO dissolved in the electrolyte was further removed by Ar bubbling for 30 min. After the stripping, supplementary cyclic voltammograms were recorded to check the complete removal of the adsorbate. Comparative CO stripping voltammograms were recorded before and after the spontaneous deposition step.

MOR and EOR were studied by cyclic voltammetry in 0.5 M H_2SO_4 with 1.0 M CH_3OH or 1.0 M CH_3CH_2OH. Each solution was previously deaerated by Ar sparging for 30 min and the gas flow was passed over the electrolyte during the potential cycling. The electrode was firstly cycled in deaerated 0.5 M H_2SO_4 and then, it was washed with Millipore Milli-Q water, dried, and transferred to the cell containing the corresponding deaerated acidic alcohol solution. Cyclic voltammograms between 0.00 and 0.65 V at 0.02 V s^{-1} and 25.0 °C were recorded.

2.4. Spontaneous deposition

The preparation of the Ru-modified Pt/C electrocatalysts (Ru(Pt)/C) was made by immersing the thin-layer Pt/C electrodes in deaerated X M $RuCl_3$ with 0.1 M $HClO_4$ solutions at 25.0 °C, with $X = 1.0 \times 10^{-4}$–1.0×10^{-2} M, for a time between 60 and 1.8×10^4 s. The $RuCl_3/HClO_4$ solutions were left aging for at least a week to facilitate the formation of aqueous Ru complexes, which were qualitatively examined by UV–visible spectroscopy using a UV-1800 Shimadzu spectrophotometer. Previous to the deposition step, the electrode was subjected to potential cycling in deaerated 0.5 M H_2SO_4 and then, washed with ultrapure water, carefully dried, and introduced in the $RuCl_3/HClO_4$ solution. After the surface modification, the resulting electrodes were washed with ultrapure water, dried and positioned again in deaerated 0.5 M H_2SO_4 for the acquisition of a new cyclic voltammogram routine. The coverage by Ru species of the Ru(Pt)/C electrocatalysts (θ) was calculated from Eq. (1) [30,33]:

$$\theta = \frac{Q_{H,0} - Q_{H,1}}{Q_{H,0}} \quad (1)$$

where $Q_{H,0}$ and $Q_{H,1}$ are the charge involved in the monoatomic hydrogen adsorption and desorption processes (with subtraction of the double layer contribution) before and after the spontaneous deposition process, respectively. The coverage of the electrocatalyst was stable with the potential cycling and reproducible under the same experimental conditions, achieving values between $\theta = 0.00$ and $\theta = 0.62$. Once the coverage was determined, CO stripping and MOR and EOR measurements were performed.

3. Results and discussion

3.1. UV–visible analysis of the $RuCl_3$–$HClO_4$ solutions

Spectrophotometric measurements were carried out on fresh and aged $RuCl_3$ solutions to characterize the nature of the Ru complexes and their evolution with time, which were interpreted from the spectral data reported in literature [34–39]. As an example, the results for the as-prepared and 1-month aged 8.0×10^{-3} M $RuCl_3$ + 0.1 M $HClO_4$ solution are depicted in Fig. 1. The UV–vis spectrum of the as-prepared solution (spectrum *a*) showed absorption bands at $\lambda_1 = 225$ nm, $\lambda_2 = 260$ nm, $\lambda_3 = 392$ nm and $\lambda_4 = 469$ nm. The first and the third bands can be attributed to the $[Ru(H_2O)_6]^{3+}$ complex. Thus, the signal at $\lambda_1 = 225$ nm is caused by a charge-transfer transition, whereas the signal at $\lambda_3 = 392$ nm is originated by a spin-allowed d–d transition [38]. The band at $\lambda_4 = 469$ nm is typically assigned to the RuO_4^{2-} species [31], but since this anion is unstable in acid solutions [36], this peak is proposed to be related to the early formation of $[RuO(H_2O)_4]^{2+}$, i.e. Ru (IV) as ruthenyle, which is the most characteristic Ru species in $HClO_4$ solutions [37,39]. This assumption is supported by the weak band observed at $\lambda_2 = 260$ nm, caused by generic Ru (IV) species [34].

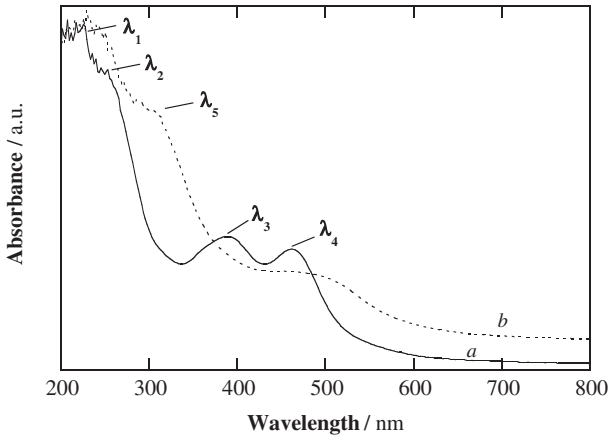

Fig. 1. UV–visible spectra of (*a*) as-prepared and (*b*) 1-month aged 8.0×10^{-3} M $RuCl_3$ + 0.1 M $HClO_4$ solution, showing the absorption bands λ_1, λ_2, λ_3, λ_4 and λ_5.

A different UV–vis spectrum can be observed for the 1-month aged solution in Fig. 1 (spectrum b). The band at $\lambda_3 = 392$ nm disappears, a new signal at $\lambda_5 \approx 300$ nm appears and the original band at $\lambda_4 = 469$ nm becomes wider between 430 and 500 nm. The more logical explanation for the disappearance of λ_3 is the complete removal of the $[Ru(H_2O)_6]^{3+}$ complex, either by formation of new Ru (III) complexes or by oxidation to Ru species of higher oxidation states. Both hypothesis are plausible by the apparition of the absorption band at $\lambda_5 \approx 300$ nm, which could be due to the contribution of $[RuO(H_2O)_4]^{2+}$ [37], $[RuCl(H_2O)_5]^{2+}$ [38], $[RuCl_2(H_2O)_4]^{+}$ [34] and perruthenate (RuO_4^-) [36], species. The presence of RuO_4^- would also cause the expansion of the band at $\lambda_4 = 469$ nm [30]. Despite the large variety of possible Ru complexes/ions, $[RuO(H_2O)_4]^{2+}$ can be considered as the main Ru species involved in the spontaneous deposition from aged $RuCl_3$ solutions [27], although the deposition from Ru (III) complexes or RuO_4^- is also plausible [30].

3.2. Cyclic voltammetry in 0.5 M H_2SO_4

The cyclic voltammograms of the Ru(Pt)/C electrocatalyst in deaerated 0.5 M H_2SO_4 are highlighted in Fig. 2, with coverages in the range 0.00–0.62. The most characteristic features when increasing θ are: (i) the decrease of the charge involved in the hydrogen adsorption/desorption ($H_{ads/des}$) reactions between 0.00

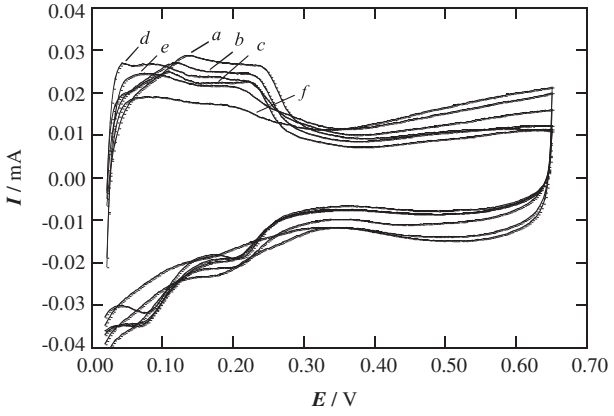

Fig. 2. Cyclic voltammograms of the Ru(Pt)/C electrocatalysts prepared through spontaneous deposition with coverage θ: (*a*) 0.00, (*b*) 0.03, (*c*) 0.14, (*d*) 0.27, (*e*) 0.44 (*d*) $\theta = 0.62$ in Ar-sparged 0.5 M H_2SO_4 at 0.02 V s^{-1} and 25.0 °C. Pt load of 30 μg cm^{-2}.

and 0.30 V and (ii) the increase of the double layer charge between 0.30 and 0.65 V. The first change is caused by the incorporation of Ru species on the surface of the Pt nanoparticles, because they are significantly less active than Pt for hydrogen adsorption/desorption [40]. On the other hand, the increase of the double layer charge is another indication of the modification of the Pt/C specimen through Ru spontaneous deposition. It has been reported that the double layer charge depends linearly on the Ru atomic fraction on Pt–Ru alloyed electrocatalysts [9]. This behavior can be explained by the pseudocapacitive behavior related to the formation of hydroxylated species on Ru atoms (Ru–OH) and/or on hydrous RuO_2 (RuO_xH_y) [7,41]. However, the charge related to the double layer cannot be used to determine the coverage of Pt by Ru species, because (bi)-sulfate anions are also adsorbed/desorbed on Pt at this potential region ($E = 0.55$ V [42]). For this reason, the estimation of the global coverage θ was made from the variation of the $H_{ads/des}$ charge, as suggested previously [30,33].

The influence of the concentration of $RuCl_3$ in 0.1 M $HClO_4$ on θ was analyzed by performing spontaneous deposition for concentrations of Ru salt (C_{Ru}) between 1.0×10^{-4} and 8.0×10^{-3} M at a fixed exposition time (1800 s). Fig. 3 presents the good linear correlation between θ and log C_{Ru} (correlation coefficient $r = 0.9986$), suggesting that the adsorption of the Ru complexes on the Pt surface obeys a Temkin isotherm, i.e., the adsorption energy changes linearly with the coverage and Eq. (2) is verified [43]:

$$\theta = k + \frac{2.3}{f}\log C_{Ru} \quad (2)$$

where k is a constant and f is the so-called inhomogeneity factor that is related to the distribution of the different adsorption sites with respect to the adsorption energy on the heterogeneous adsorbent surface. From the slope of the plot of Fig. 3 ($m = 0.21$), a f value of 11 is obtained. The excellent agreement of this value with that reported for the adsorption of organic molecules, as methanol or formic acid ($f \approx 12$) or even for hydrogen adsorption on Pt surfaces ($f \approx 14$) [44], supports the use of the above Temkin isotherm for modeling the spontaneous deposition of Ru species on Pt nanoparticles.

The dependence of θ on the duration of the deposition process was assessed at different times between 300 and 1.8×10^4 s in 8.0×10^{-3} M $RuCl_3$ + 0.1 M $HClO_4$ solutions. The coverage rate $v = d\theta/dt$ was analyzed by the Roginsky–Zeldovich–Elovich (RZE) expression given by Eq. (3), which is valid when the adsorption process takes place on an uniformly heterogeneous surface [44,45]:

$$v = \frac{d\theta}{dt} = k' C_{Ru} \exp(-\alpha f \theta) \quad (3)$$

In Eq. (3), k' is the adsorption constant and α is the transfer coefficient of the process, which takes a value between 0 and 1. According to the RZE expression, the rate of covering decreases exponentially with increasing coverage. The integrated form of Eq. (3) is given by Eq. (4) [44]:

$$\theta = \frac{2.3}{b}\log(ab) + \frac{2.3}{b}\log t \quad (4)$$

where $a = k' C_{Ru}$ and $b = \alpha f$. Thus, a linear dependence of θ on the logarithm of deposition time (t) is expected, with a slope (p) = 2.3/b and a Y-intercept (Y_θ) = 2.3/b log (ab). The linear θ vs log t plot presented in Fig. 4 ($r = 0.9841$) agrees with the prediction of the RZE equation. From the slope $p = 0.20$, $b = 12$ is obtained. Taking $f = 11$ as calculated above, a value of α close to 1.0 is found, which is quite reasonable and in agreement with the adsorption kinetics based on the RZE model. From Fig. 4, it can be also determined that $Y_\theta = -0.20$, leading to $a = 8.0 \times 10^{-3}$ s^{-1}. Taking into account that $C_{Ru} = 8.0 \times 10^{-3}$ M, $k' = 1.0$ M^{-1} s^{-1}. Note that this analysis excludes the nature of the Ru species deposited through spontaneous deposition, but it gives an interesting information about the parameters that affect particular coverages.

3.3. CO stripping voltammetry in 0.5 M H_2SO_4

The tolerance towards the CO poisoning of the modified Ru(Pt)/C electrocatalysts was tested from CO stripping trials in 0.5 M H_2SO_4. Fig. 5 displays the voltammograms recorded for different Ru(Pt)/C electrocatalysts (curves *a–f*) with θ between 0.00 and 0.41. The anodic peak is caused by the bi-electronic oxidation of the adsorbed CO monolayer on the electrocatalyst surface by reaction (5):

$$CO_{ads} + H_2O \rightarrow CO_2 + 2H^+ + 2e^- \quad (5)$$

As can be observed in Fig. 5, the incorporation of Ru species on the surface of the Pt nanoparticles changes the onset potential for the CO oxidation to a more negative value, with an average shift of $\Delta E = 0.20$ V for the Ru(Pt)/C specimens compared to the untreated

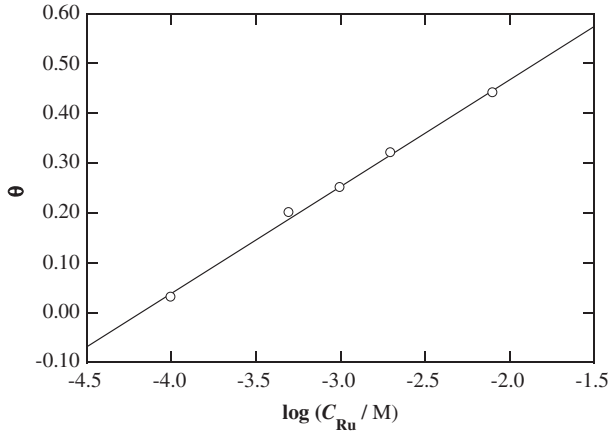

Fig. 3. Coverage of Pt by Ru species as a function of the logarithm of the $RuCl_3$ concentration in 0.1 M $HClO_4$ solutions used for the spontaneous deposition. Data obtained from cyclic voltammograms recorded as shown in Fig. 2.

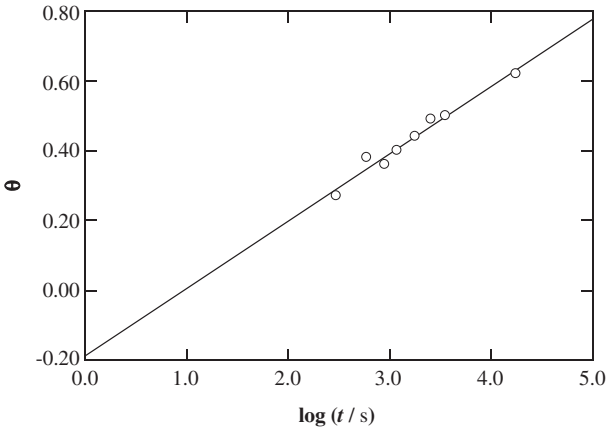

Fig. 4. Coverage of Pt by Ru species versus the logarithm of the immersion time of the electrode in 8.0×10^{-3} M $RuCl_3$ + 0.1 M $HClO_4$ solution. Coverage calculated from cyclic voltammograms recorded under the same conditions of Fig. 2.

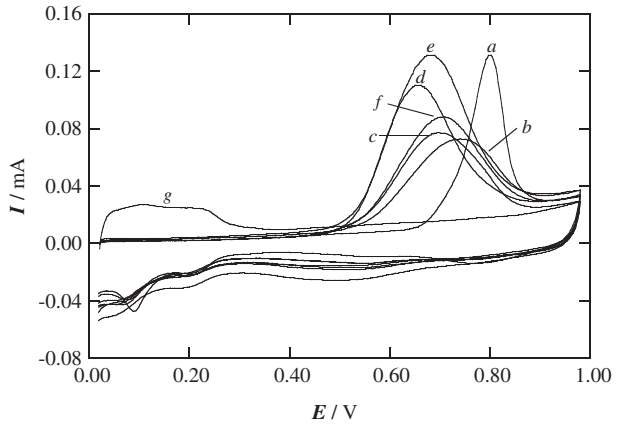

Fig. 5. Cyclic voltammograms for CO stripping on the Ru(Pt)/C electrocatalysts prepared with θ: (*a*) 0.00, (*b*) 0.03, (*c*) 0.14, (*d*) 0.22, (*e*) 0.32 and (*f*) 0.41 in Ar-sparged 0.5 M H_2SO_4 at 0.02 V s^{-1} and 25.0 °C. CO was previously adsorbed during 15 min at 0.01 V and Ar was later sparged for 30 min. (*g*) Cyclic voltammogram for the Ru(Pt)/C electrocatalyst with $\theta = 0.41$ without adsorbed CO. Catalyst load of 30 μg Pt cm^{-2}.

Pt/C electrocatalyst. This then indicates that a better CO tolerance is achieved when preparing Ru(Pt)/C electrocatalysts via spontaneous deposition on Pt/C ones. A similar trend in the CO oxidation overpotential was previously reported for a commercial alloyed Pt–Ru/C electrocatalyst [46]. The better tolerance with respect to the CO poisoning in both cases is due to the action of hydroxylated Ru species which react with the adsorbed CO moieties that block the Pt active sites.

Another interesting fact depicted in the cyclic voltammograms of Fig. 5 is the presence of a unique CO stripping peak in all cases. This behavior differs from the two contributions reported for the CO oxidation on Ru-decorated macroscopic Pt surfaces [47], one corresponding to the Pt sites close to the Ru moieties and the other one related to the Pt sites separated from the deposited Ru species. Thus, the presence of a single peak on the Ru(Pt)/C electrocatalysts, as typically obtained for Pt–Ru alloys [23,48], indicates an homogeneous distribution of the Ru species on the original Pt nanoparticles.

The *I*–*E* curves of Fig. 5 also show the change of two main parameters with θ: (i) the CO stripping peak potential ($E_{p,CO}$) and (ii) the charge involved in the anodic process (Q_{CO}). The latter is connected to the electrochemical active surface area (ECSA) of the electrocatalyst, considering that a charge of 420 μC cm^{-2} is needed for the oxidation of a CO monolayer [48]. The analysis of $E_{p,CO}$ and the variation of ECSA with respect to the untreated Pt/C electrocatalyst, expressed as percentage (ΔECSA), in front of the coverage, are presented in Fig. 6a and b, respectively. ΔECSA values were calculated according to the expression $\Delta ECSA = ((Q_{CO,1} - Q_{CO,0})/Q_{CO,0}) \times 100$, where $Q_{CO,0}$ and $Q_{CO,1}$ are the charges for CO stripping before and after the spontaneous deposition, respectively.

Fig. 6a evidences that $E_{p,CO}$ reaches its minimum value for θ about 0.22, where the electrocatalyst attains the best performance for CO oxidation, with a reduction of the peak potential of 0.16 V. At this coverage, the closest approach between adsorbed CO_{ads} and OH_{ad} species is expected, thus making more effective the bifunctional mechanism. Note that this coverage is significantly smaller than $\theta = 0.50$, which could be initially suggested from the bifunctional mechanism on Pt–Ru alloys (a CO molecule on a Pt atom close to a Ru–OH moiety). However, this assumption is only valid when Ru metal is considered, and, consequently, our result of $\theta = 0.22$ could be due to the deposition of other Ru species like RuO_xH_y, which have a promotional effect for CO oxidation even greater than metallic Ru [26].

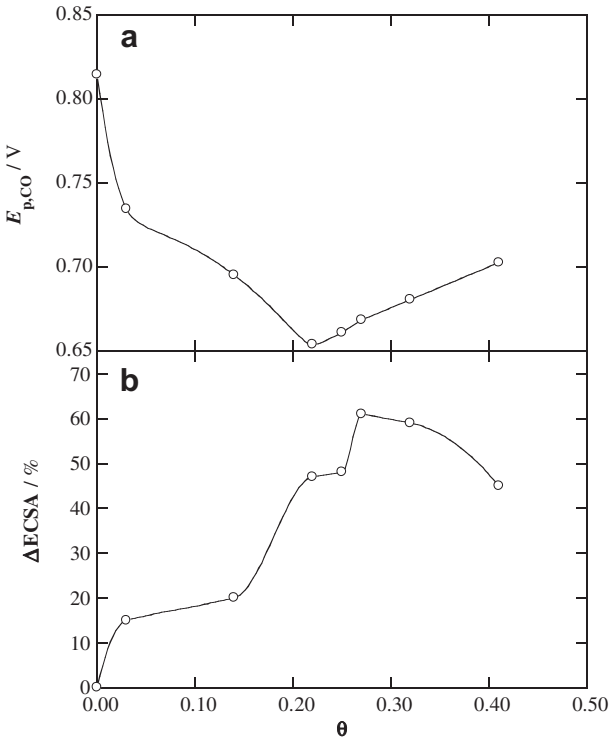

Fig. 6. (a) Anodic peak potential for CO stripping and (b) electrochemical active surface area (ECSA) variation with θ. Data obtained from cyclic voltammograms for the CO oxidation on Ru(Pt)/C electrocatalysts recorded in the same conditions as in Fig. 5.

Fig. 6b shows a regular increase of the active surface area up to achieve a maximum ΔECSA = 60% at θ about 0.27, which is further reduced for higher coverages. This maximum can be related to the optimum surface composition originating the best synergistic effect between the Pt sites and the incorporated Ru species. Note also that this value is close to $\theta = 0.22$, which corresponds to the lowest $E_{p,CO}$. The increase in the ΔECSA for low coverages takes place together with the reduction in the charge for the hydrogen adsorption/desorption, and therefore, it has to be explained by the participation of other species different from Pt, also able to adsorb CO. This different species is most probably Ru metal, produced by partial reduction during CO adsorption, of the Ru oxides produced by spontaneous deposition. It is known that CO is not chemisorbed on Ru oxides [24] and that CO molecules are bonded linearly to Pt atoms with a conversion factor of 420 μC cm^{-2}, whereas for the bi-electronic CO oxidation of Ru (001), this factor rises to 506 μC cm^{-2} [40,49]. It can be argued that a non-faradaic charge could contribute to the Q_{CO} calculation at each coverage [50,51], but this contribution should not be significant in our case because curve *g* in Fig. 5 shows a negligible capacitive contribution in front of Q_{CO} at high θ values. In addition, the partial reduction of the Ru oxides produced by spontaneous deposition at low coverages was also claimed by Chrzanowski and Wieckowski from CV studies on single crystal Pt faces [27].

According to these arguments, for coverages greater than about 0.27, the ECSA decreases and the peak potential of CO stripping moves in the positive direction because the amount of Ru oxides spontaneously deposited overcompensate the free Pt sites and, in addition, such oxides are less reducible. The non-reducible character of the Ru oxides produced by spontaneous deposition with high coverages was also invoked by Maillard et al. from CV studies [31].

In short, the model explaining the present results should consider the formation of Ru oxides such as RuO_xH_y during the

spontaneous deposition. Some Ru oxides are partially reducible at low coverages (smaller than about 0.25), so that Ru and RuO_xH_y could contribute to the promotional effect for CO oxidation. In contrast, for coverages higher than about 0.25, Ru oxides become non-reducible, although RuO_xH_y would also contribute to the promotional effect for CO oxidation. Then, the increasing amounts of non-reducible deposited oxides would block more Pt active sites so that such a promotional effect decreases.

3.4. Tafel analysis of CO oxidation on Ru(Pt)/C

The E vs. log I plots for the CO oxidation on the untreated electrocatalyst, curve *a*, and on Ru(Pt)/C specimens with coverage in the range 0.14–0.41, curves *b*–*e*, were built up using the I–E data collected in the lower overpotential region close to the onset potential (i.e. 0.65–0.75 and 0.50–0.60 V for Pt/C and Ru(Pt)/C, respectively). From these plots, shown in Fig. 7a, the apparent Tafel slopes, b_{CO}, were determined in the linear regions with $r \geq 0.99$ and the variation of these apparent Tafel slopes with θ have been depicted in Fig. 7b. For untreated Pt/C, b_{CO} was close to 120 mV, in agreement with the theoretical value for a multistep reaction with the first electron transfer being the rate-determining step (rds), the adsorbed intermediates following a Langmuir isotherm [52]. Christensen et al. [5] proposed the direct oxidation of the adsorbed CO molecules by water (Eley–Rideal mechanism) from reaction (6), followed by an oxidation to generate CO_2 via reaction (7):

$$Pt{-}CO + H_2O \rightarrow Pt{-}CO_2H_{ads} + H^+ + e^- \quad (6)$$

$$Pt{-}CO_2H_{ads} \rightarrow Pt + CO_2 + H^+ + e^- \quad (7)$$

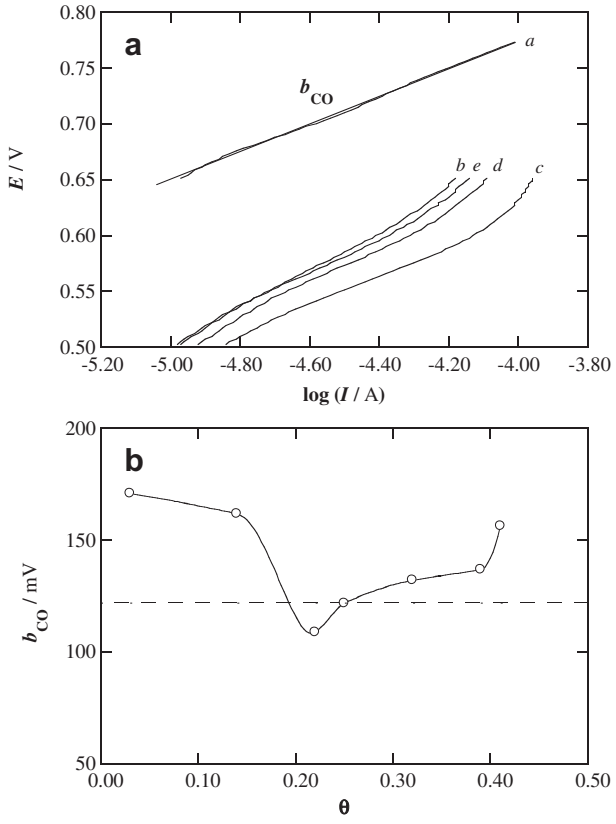

Fig. 7. (a) Tafel plots for the CO oxidation on Ru(Pt)/C electrocatalysts with θ: (*a*) 0.00, (*b*) 0.14, (*c*) 0.25, (*d*) 0.32 and (*e*) 0.41. (b) Apparent Tafel slope for CO oxidation as a function of θ. Data collected from polarization curves obtained from CO stripping experiments made as in Fig. 5.

In contrast, Seland et al. [10] proposed the presence of hydroxylated Pt species formed by water discharge on Pt free sites through step (8) and a consecutive Langmuir–Hinshelwood oxidation step from reaction (9):

$$Pt + H_2O \rightarrow Pt{-}OH + H^+ + e^- \quad (8)$$

$$Pt{-}CO + Pt{-}OH \rightarrow 2Pt + CO_2 + H^+ + e^- \quad (9)$$

The Tafel slope of 120 mV for the Pt/C electrocatalyst could then be due to steps (6) or (8) as the rds of the mechanism. On the other hand, Fig. 7b shows that for the Ru(Pt)/C electrocatalysts, the Tafel slope presented a minimum of about 110 mV at $\theta = 0.22$, whereas higher values of about 160–170 mV were obtained for $\theta = 0.03$–0.14 and a gradual increase from 120 to 160 mV was found from $\theta = 0.25$ to $\theta = 0.41$. As previously suggested [26,41], the Ru-modified specimens could be oxidized to hydroxylated Ru moieties ($RuO_xH_y(OH)$) through reaction (10), which could further react with the adsorbed CO on the Pt active sites by reaction (11):

$$RuO_xH_y + H_2O \rightarrow RuO_xH_y(OH) + H^+ + e^- \quad (10)$$

$$RuO_xH_y(OH) + Pt{-}CO \rightarrow RuO_xH_y + Pt + CO_2 + H^+ + e^- \quad (11)$$

Assuming reaction (10) as the rds, the average Tafel slope for the Ru(Pt)/C electrocatalysts is expected to be ~140 mV [12,53]. However, this step takes place simultaneously to the slow reaction (11), which can be related to lower apparent Tafel slopes of 110–120 mV. As the variation of the Tafel slope with the coverage follows the same trend as the CO stripping peak potential in Fig. 6a and a minimum Tafel slope of about 110 mV is found for the same θ of 0.22, it is suggested that at this coverage the CO oxidation reaction is kinetically more favored.

3.5. Methanol and ethanol oxidation reaction on Ru(Pt)/C

Fig. 8a presents the anodic scans obtained for the MOR in 0.5 M H_2SO_4 + 1.0 M CH_3OH using Ru(Pt)/C electrocatalysts prepared with θ between 0.00 and 0.62. The overall reaction can be written as follows:

$$CH_3OH + H_2O \rightarrow CO_2 + 6H^+ + 6e^- \quad (12)$$

A general decay of 0.10 V in the onset potential can be observed for the Ru-modified specimens (curves *b*–*e*) in comparison to the untreated Pt/C electrocatalyst (curve *a*), indicating a promotional effect of the MOR as a result of the spontaneous deposition. Moreover, the MOR current density (j_{MOR}) is found markedly dependent on the coverage. As can be seen in the inset panel of Fig. 8a, j_{MOR} reaches a maximum at $\theta \approx 0.25$ for the three selected potentials. At 0.50 V, for example, this maximum value is about 3 times higher than the j_{MOR} of the Pt/C electrocatalyst. This greater performance is then achieved by the incorporation of Ru species on the Pt surface, as detected in the CO stripping experiments. Note in addition that the same optimum coverage as for the latter is obtained, thus indicating that CO is an intermediate involved in the rds corresponding the MOR mechanism. The decrease of j_{MOR} at $\theta > 0.25$ would be caused by a blocking effect of the Ru deposits on the Pt active sites, as discussed above for the CO oxidation.

The behavior of the Ru(Pt)/C electrocatalysts in front of the EOR was evaluated in the same way using a 0.5 M H_2SO_4 + 1.0 M CH_3CH_2OH. The corresponding anodic voltammograms for the Ru-modified electrocatalysts with coverages between 0.00 and 0.59 are depicted in Fig. 8b. In this case, the overall EOR process can be expressed as follows:

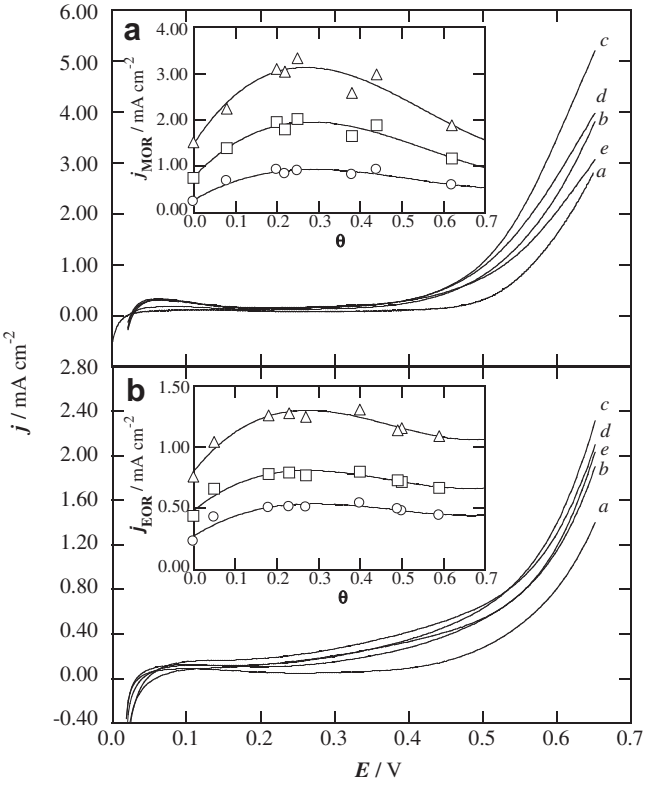

Fig. 8. (a) Cyclic voltammograms (only the anodic swept is shown) for the methanol oxidation reaction (MOR) on the Ru(Pt)/C electrocatalyst with θ: (*a*) 0.00, (*b*) 0.08, (*c*) 0.25, (*d*) 0.40 and (*e*) 0.62. The inset panel shows the MOR current density at (○) 0.50 V, (□) 0.55 V and (△) 0.60 V vs θ. Data obtained in 0.5 M H_2SO_4 + 1.0 M CH_3OH at 0.02 V s^{-1} and 25.0 °C. (b) Polarization curves (only anodic scans) corresponding to the ethanol oxidation reaction (EOR) on the same electrocatalyst with θ: (*a*) 0.00, (*b*) 0.05, (*c*) 0.23, (*d*) 0.49 and (*e*) 0.59. The inset panel presents the change of EOR current density at (○) 0.50 V, (□) 0.55 V and (△) 0.60 V with θ. Data obtained in 0.5 M H_2SO_4 + 1.0 M CH_3CH_2OH at 0.02 V s^{-1} and 25.0 °C.

$$CH_3CH_2OH + 3H_2O \rightarrow 2CO_2 + 12H^+ + 12e^- \quad (13)$$

As in the case of the MOR, a considerable reduction of the onset potential close to 0.20 V is achieved when the EOR takes places on the Ru-modified electrodes. The inset panel of Fig. 8b also shows that the EOR current density at low overpotential (j_{EOR}) reaches a maximum for $\theta \approx 0.20-0.30$ in all the potentials selected. The similar value of this coverage to that found for the MOR suggests that CO/CH_xO generation takes place during the EOR, in agreement with Gomes et al. [16], who used Fourier transform infrared spectroscopy (FTIR) on low-index Pt surfaces. One can then suppose that the hydroxylated Ru species present in the Ru(Pt)/C electrocatalysts are also involved in the ethanol electrooxidation pathway. Note that the EOR leads to the formation of not only CO_2 on Pt-based electrocatalysts, but also to products like CH_3CHO (2-electron process) and CH_3COOH (4-electron process) [14,17]. According to Camara et al. [14], the acetic-acid production is enhanced via oxidation of acetaldehyde in Pt–Ru alloys compared to Pt electrocatalysts, with only a minimal production of CO_2 (5%). Therefore, it is reasonable to assume that up to θ ca. 0.25, increasing amounts of Ru species gradually promote the EOR by the oxidation of intermediates with the help of the hydroxylated Ru moieties, thus resulting in an increase of j_{EOR}. The progressive inhibition of the EOR for $\theta > 0.25$ can again be related to the blocking effect of larger amounts of Ru deposits on the active sites for the alcohol oxidation.

3.6. Tafel analysis of MOR and EOR on Ru(Pt)/C

The *E* vs. log *I* plots for the MOR on the modified Ru(Pt)/C electrocatalysts are shown in Fig. 9a. From these plots, the Tafel slopes, b_{MOR}, were determined in the linear regions with $r \geq 0.99$ and depicted in the inset of the same figure. As can be observed, the incorporation of Ru species on the electrocatalyst causes a gradual increase of the Tafel slope with coverage, being $b_{MOR} = 230$ mV at $\theta = 0.62$, which is almost twice the value of 123 mV obtained for the untreated Pt/C electrocatalyst. The Tafel slope of ca. 120 mV at $\theta = 0.00$ agrees with the theoretically expected value for a first electron transfer being the rds and the adsorption of intermediates under Langmuir conditions. A plausible mechanism for the MOR is initiated by the adsorption of methanol on Pt active sites from reaction (14), followed by consecutive dehydrogenation steps until the adsorbed CO is formed via reactions (15) and (16) [10]:

$$Pt + CH_3OH \rightarrow Pt{-}CH_3OH_{ads} \quad (14)$$

$$Pt{-}CH_3OH_{ads} \rightarrow Pt{-}CH_xO_{ads} + (4-x)H^+ + (4-x)e^- \quad (x = 1,2,3) \quad (15)$$

$$Pt{-}CHO_{ads} \rightarrow Pt{-}CO + H^+ + e^- \quad (16)$$

The adsorbed CO would then be oxidized following the reaction pathways described above, so that, reaction (6) or (8) could be the rds of the MOR taking into account that the 4-electron methanol

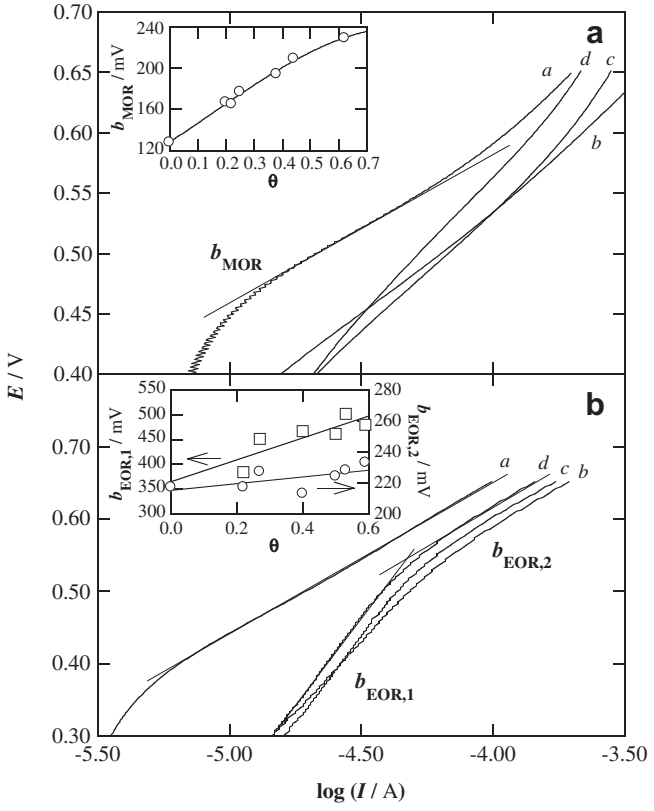

Fig. 9. (a) Tafel plots for the MOR on the Ru(Pt)/C electrocatalysts with θ: (*a*) 0.00, (*b*) 0.22, (*c*) 0.38 and (*d*) 0.62. The inset panel presents the apparent Tafel slope for the MOR (b_{MOR}) as a function of θ. (b) Tafel plots for the EOR on the on the same electrocatalysts with θ: (*a*) 0.00, (*b*) 0.22, (*c*) 0.40 and (*d*) 0.58. The inset panel shows the apparent Tafel slopes for the EOR at the low overpotential ($b_{MOR,1}$) and the high overpotential ($b_{MOR,2}$) regions plotted vs θ. MOR and EOR polarization curves were obtained under the same conditions of Fig. 8.

dehydrogenation process is a faster pathway. In contrast, the continuous increase of the Tafel slope with θ could be related to the introduction of Ru deposits that generate hydroxylated species with a strong potential dependence with coverage that cannot be simply interpreted from Butler–Volmer equation [52]. A similar trend was described by Sieben et al. when analyzing the MOR on supported Pt and Pt–Ru nanoparticles prepared by potentiostatic electrodeposition [11]. A similar and high Tafel slope of ~200 mV, strongly dependent on the temperature and the coverage, was also found for the MOR on an alloyed Pt–Ru/C electrocatalyst, reaction (11) being proposed as the rds [12]. Moreover, the adsorption of intermediates ($Pt–CH_3OH_{ads}$, $Pt–CH_xO$, Pt–CO, $RuO_xH_y(OH)$) under Temkin conditions could increase the Tafel slope for the MOR on the Ru(Pt)/C electrocatalysts twice the ordinary value of 120 mV [52].

Fig. 9b depicts the E vs. log I plots for the EOR on Ru(Pt)/C electrocatalysts with θ from 0.00 to 0.59. While the unmodified specimen presents a single Tafel plot in the potential region of 0.40–0.60 V, the Ru-modified specimens show two anomalous Tafel slopes, $b_{EOR,1} = 380–500$ mV in the lower overpotential region of 0.30–0.50 V and $b_{EOR,2,} = 220–230$ mV in the higher overpotential region of 0.50–0.60 V. All these Tafel slopes were determined from the corresponding linear regions with $r \geq 0.99$. The latter slope approaches the value for the untreated Pt/C electrocatalyst. Both $b_{EOR,1}$ and $b_{EOR,2}$ vaguely increase with coverage, as can be seen in the inset of Fig. 9b. The ratio between the high and the low Tafel slope was maintained equal to 1.9 ± 0.2 in the entire range of coverage analyzed. As in the case of the MOR, these Tafel slopes have not the usual meaning extracted from formal Electrodics analysis, since the EOR takes place on a changing Ru(Pt) surface–electrolyte interface with continuous generation of intermediate species. Note that a b_{EOR} as high as 300 mV was reported by Otomo et al. [19] for the EOR on a carbon-supported Pt electrocatalyst, whereas Du et al. [15] found a slope of 257 mV dec^{-1} for a Pt–Ru/C specimen. Taking into account the detected intermediates in the EOR [16,17,20], the following mechanism has been proposed. It starts with the chemisorption of ethanol on Pt active sites via reaction (17), which is subsequently oxidized to acetaldehyde by reaction (18). The adsorbed acetaldehyde can react with Pt and/or hydroxylated Ru species to yield acetic acid from reaction (19), where OH_{ads} represents the species formed in reactions (8) or (10).

$$Pt + CH_3CH_2OH \rightarrow Pt–CH_3CH_2OH_{ads} \quad (17)$$

$$Pt–CH_3CH_2OH_{ads} \rightarrow Pt–CH_3CHO_{ads} + 2H^+ + 2e^- \quad (18)$$

$$Pt–CH_3CHO_{ads} + OH_{ads} \rightarrow Pt–CH_3COOH_{ads} + H^+ + e^- \quad (19)$$

The rupture of the C–C bond could be an alternative pathway to generate acetyl radical from reaction (20), which suffers a homolytic cleavage to give carbon monoxide and methyl radical by reaction (21). The CO thus formed is further oxidized to CO_2 by the action of water from reaction (6) or by OH_{ads} moieties via reaction (9) and/or (11). The methyl radical is removed by reaction with adsorbed hydrogen leading to methane by reaction (22) [17].

$$Pt–CH_3CHO_{ads} \rightarrow Pt–CH_3CO_{ads} + H^+ + e^- \quad (20)$$

$$Pt–CH_3CO_{ads} + Pt \rightarrow Pt–CO + Pt–CH_{3,ads} \quad (21)$$

$$Pt–CH_{3,ads} + Pt–H \rightarrow 2Pt + CH_4 \quad (22)$$

The existence of two Tafel slopes for the EOR and their dependence on the coverage could be related to a change of the rds on the Ru(Pt)/C electrocatalysts when the potential is increased. The abnormal high value of $b_{EOR,1}$ may be assigned to a rds involving a chemical step without electron transfer such as the formation of CO adsorbed on Pt active sites by reaction (21) [52]. The Tafel region with lower $b_{EOR,2}$ may then be associated with the CO oxidation as the slow step of the EOR pathway, following reactions (6)–(9) or (10) and (11) for Pt/C or Ru(Pt)/C electrocatalysts, respectively, as commented for the MOR. This is supported by the similar $b_{EOR,2}$ and b_{MOR} values obtained at the same potential region where they appear.

4. Conclusions

Ru(Pt)/C electrocatalysts with controlled coverage of Pt nanoparticles by Ru species were synthesized using the spontaneous deposition technique. The deposition from Ru aqueous complexes, mainly containing $[RuO(H_2O)_4]^{2+}$ species, was studied by cyclic voltammetry and could be adjusted to a Temkin adsorption isotherm and to an RZE kinetics. The CO stripping experiments showed the maximum catalytic activity for the Ru(Pt)/C electrocatalysts when $\theta = 0.20–0.30$, owing to the reduction of the overpotential and the increase of the ECSA. The introduction of Ru species mainly as RuO_xH_y (hydrated RuO_2) is proposed to explain its promotional effect, based on the participation of hydroxylated Ru species on the CO removal. Similar Tafel slopes, close to 120 mV, were found for the CO oxidation on the Ru(Pt)/C specimens with a minimum Tafel slope of 110 mV for the most favorable coverage, indicating the first electron transfer as the rds. An enhancement of the MOR and EOR and a similar optimum coverage close to 0.25 was determined for the Ru(Pt)/C electrocatalysts, suggesting the formation of CH_xO/CO as adsorbed intermediates and the participation of $RuO_xH_y(OH)$ species in the oxidation pathway of both alcohols. The Tafel slopes varied with the coverage by Ru species. For the MOR, a progressive increase of the Tafel slope with θ from an initial value of about 120 mV up to a final one of about 230 mV was found, being ascribed to the action of the generated adsorbed intermediates under Temkin conditions in the CO oxidation as the rds. An analogous evolution of the Tafel slopes with the coverage was obtained for the EOR, but presenting double Tafel slope behavior, explained assuming a change of the rds from a chemical step without electron transfer to the CO oxidation removal. The present work shows the viability of the spontaneous deposition as suitable technique for the preparation of CO tolerant and active MOR/EOR Ru(Pt)/C electrocatalysts as an alternative to the more utilized Pt–Ru alloy systems.

Acknowledgments

The authors thank the financial support from the project NAN2004-09333-C05-03 and the FPU fellowship MEC received by A. Velázquez-Palenzuela to do this work from the Spanish MEC (Ministerio de Educación y Ciencia). This work is dedicated to the memory of Amado Velázquez Méndez.

References

[1] F. Alcaide, P.L. Cabot, E. Brillas, J. Power Sources 153 (2006) 47–60.
[2] W. Vielstich, A. Lamm, H.A. Gasteiger, Handbook of Fuel Cells-fundamentals, Technology and Applications: Rotating Thin Film Method for Supported Catalysis, John Wiley & Sons, New York, 2003 (chapter 22), pp. 316–333.
[3] T. Iwasita, Handbook of Fuel Cells-fundamentals, Technology and Applications: Methanol and CO Electrooxidation, John Wiley & Sons, New York, 2003 (chapter 41), pp. 603–624.
[4] A.S. Arico, P.L. Antonucci, E. Modica, V. Baglio, H. Kim, V. Antonucci, Electrochim. Acta 47 (2002) 3723–3732.
[5] P.A. Christensen, A. Hamnett, G.L. Troughton, J. Electroanal. Chem. 362 (1993) 207–218.
[6] T. Frelink, W. Visscher, J.A.R. Van Veen, Langmuir 12 (1996) 3702–3708.

[7] H.A. Gasteiger, N. Markovic, P.N. Ross Jr., E.J. Cairns, J. Electrochem. Soc. 141 (1994) 1795–1803.
[8] S.L. Gojković, T.R. Vidakovi&cacute, Electrochim. Acta 47 (2001) 633–642.
[9] S.L. Gojković, T.R. Vidaković, D.R. Durovi&cacute, Electrochim. Acta 48 (2003) 3607–3614.
[10] F. Seland, R. Tunold, D.A. Harrington, Electrochim. Acta 51 (2006) 3827–3840.
[11] J.M. Sieben, M.M.E. Duarte, C.E. Mayer, J. Appl. Electrochem. 38 (2008) 483–490.
[12] A. Velázquez-Palenzuela, F. Centellas, J.A. Garrido, C. Arias, R.M. Rodríguez, E. Brillas, P.L. Cabot, J. Power Sources 196 (2011) 3503–3512.
[13] T. Vidaković, M. Christov, K. Sundmacher, J. Electroanal. Chem. 580 (2005) 105–121.
[14] G.A. Camara, R.B. de Lima, T. Iwasita, J. Electroanal. Chem. 585 (2005) 128–131.
[15] W. Du, Q. Wang, D. Saxner, N.A. Deskins, D. Su, J.E. Krzanowski, A.I. Frenkel, X. . Teng, J. Am. Chem. Soc. 133 (2011) 15172–15183.
[16] J.F. Gomes, B. Busson, A. Tadjeddine, G. Tremiliosi-Filho, Electrochim. Acta 53 (2008) 6899–6905.
[17] T. Iwasita, E. Pastor, Electrochim. Acta 39 (1994) 531–537.
[18] F.H.B. Lima, E.R. Gonzalez, Electrochim. Acta 53 (2008) 2963–2971.
[19] J. Otomo, S. Nishida, H. Takahashi, H. Nagamoto, J. Electroanal. Chem. 615 (2008) 84–90.
[20] F. Vigier, C. Coutanceau, F. Hahn, E.M. Belgsir, C. Lamy, J. Electroanal. Chem. 563 (2004) 81–89.
[21] S. Alayoglu, A.U. Nilekar, M. Mavrikakis, B. Eichhorn, Nat. Mater. 7 (2008) 333–338.
[22] J.R.C. Salgado, F. Alcaide, G. Álvarez, L. Calvillo, M.J. Lázaro, E. Pastor, J. Power Sources 195 (2010) 4022–4029.
[23] J.R.C. Salgado, J.J. Quintana, L. Calvillo, M.J. Lázaro, P.L. Cabot, I. Esparbé, E. Pastor, Phys. Chem. Chem. Phys. 10 (2008) 6796–6806.
[24] J.L. Gómez de la Fuente, M.V.M. Huerta, S. Rojas, P.H. Fernández, P. Terreros, J.L.G. Fierro, M.A. Peña, Appl. Catal. B: Environ. 88 (2009) 505–514.
[25] A. Velázquez-Palenzuela, F. Centellas, J.A. Garrido, C. Arias, R.M. Rodríguez, E. Brillas, P.L. Cabot, J. Phys. Chem. C 114 (2010) 4399–4407.
[26] D.R. Rolison, P.L. Hagans, K.E. Swider, J.W. Long, Langmuir 15 (1999) 774–779.
[27] W. Chrzanowski, A. Wieckowski, Langmuir 13 (1997) 5974–5978.
[28] T. Iwasita, H. Hoster, A. John-Anacker, W.F. Lin, W. Vielstich, Langmuir 16 (2000) 522–529.
[29] H. Kim, I.R. de Moraes, G. Tremiliosi-Filho, R. Haasch, A. Wieckowski, Surf. Sci. 474 (2001) L203–L212.
[30] J.P. MacDonald, B. Gualtieri, N. Runga, E. Teliz, C.F. Zinola, Int. J. Hydrogen Energy 33 (2008) 7048–7061.
[31] F. Maillard, F. Gloaguen, J.M. Leger, J. Appl. Electrochem. 33 (2003) 1–8.
[32] P. Waszczuk, J. Solla-Gullón, H.S. Kim, Y.Y. Tong, V. Montiel, A. Aldaz, A. Wieckowski, J. Catal. 203 (2001) 1–6.
[33] Y. Du, C. Wang, Mater. Chem. Phys. 113 (2009) 927–932.
[34] H.H. Cady, R.E. Connick, J. Am. Chem. Soc. 80 (1958) 2646–2652.
[35] R.E. Connick, D.A. Fine, J. Am. Chem. Soc. 83 (1961) 3414–3416.
[36] R.E. Connick, C.R. Urley, J. Am. Chem. Soc. 74 (1952) 5012–5015.
[37] F.P. Gortsema, J.W. Cobble, J. Am. Chem. Soc. 83 (1961) 4317–4321.
[38] Z. Harzion, G. Navon, Inorg. Chem. 19 (1980) 2236–2239.
[39] P. Wehner, J.C. Hindman, J. Am. Chem. Soc. 72 (1950) 3911–3918.
[40] H.A. Gasteiger, N.M. Markovic, P.N. Ross Jr., J. Phys. Chem. 99 (1995) 8290–8301.
[41] W. Sugimoto, K. Yokoshima, Y. Murakami, Y. Takasu, Electrochim. Acta 52 (2006) 1742–1748.
[42] I. Esparbé, E. Brillas, F. Centellas, J.A. Garrido, R.M. Rodríguez, C. Arias, P.L. Cabot, J. Power Sources 190 (2009) 201–209.
[43] O.A. Khazova, A.A. Mikhailova, A.M. Skundin, E.K. Tuseeva, A. Havránek, K. Wippermann, Fuel Cells (2002) 99–108.
[44] V.S. Bagotzky, Y.U. Vassiliev, Electrochim. Acta 11 (1966) 1439–1461.
[45] F.C. Wu, R.L. Tseng, R.S. Juang, Chem. Eng. J. 150 (2009) 366–373.
[46] A. Velázquez, F. Centellas, J.A. Garrido, C. Arias, R.M. Rodríguez, E. Brillas, P.L. Cabot, J. Power Sources 195 (2010) 710–719.
[47] J.S. Spendelow, P.K. Babu, A. Wieckowski, Curr. Opin. Solid State Mater. Sci. 9 (2005) 37–48.
[48] L. dos Santos, F. Colmati, E.R. Gonzalez, J. Power Sources 159 (2006) 869–877.
[49] O.B. Alves, H.E. Hoster, R.J. Behm, Phys. Chem. Chem. Phys. 13 (2011) 6010–6021.
[50] Z. Jusys, J. Kaiser, R.J. Behm, Electrochim. Acta 47 (2002) 3693–3706.
[51] M.J. Weaver, S.C. Chang, L.W.H. Leung, X. Jiang, M. Rubel, M. Szklarczyk, D. Zurawski, A. Wieckowski, J. Electroanal. Chem. 327 (1992) 247–260.
[52] J.O.M. Bockris, S.U.M. Khan, Surface Electrochemistry: A Molecular Level Approach, Plenum Press, New York, 2003, pp. 280–285.
[53] A. Velázquez-Palenzuela, P.L. Cabot, F. Centellas, J.A. Garrido, C. Arias, R.M. Rodríguez, E. Brillas, Int. J. Hydrogen Energy 35 (2010) 11591–11600.